Comput Mech (2012) 49:21–33
DOI 10.1007/s00466-011-0624-3

ORIGINAL PAPER

Refined *h*-adaptive finite element procedure for large deformation geotechnical problems

Mina Kardani · Majidreza Nazem · Andrew J. Abbo · Daichao Sheng · Scott W. Sloan

Received: 5 November 2010 / Accepted: 26 June 2011 / Published online: 15 July 2011

Abstract Adaptive finite element procedures automatically refine, coarsen, or relocate elements in a finite element mesh to obtain a solution with a specified accuracy. Although a significant amount of research has been devoted to adaptive finite element analysis, this method has not been widely applied to nonlinear geotechnical problems due to their complexity. In this paper, the *h*-adaptive finite element technique is employed to solve some complex geotechnical problems involving material nonlinearity and large deformations. The key components of *h*-adaptivity including robust mesh generation algorithms, error estimators and remapping procedures are discussed. This paper includes a brief literature review as well as formulation and implementation details of the *h*-adaptive technique. Finally, the method is used to solve some classical geotechnical problems and results are provided to illustrate the performance of the method.

Keywords Adaptivity · Finite elements · Large deformation · Geomechanics · *h*-Adaptive refinement

1 Introduction

The finite element method (FEM) is a robust technique for the analysis of a large number of problems in engineering where analytical solutions cannot be obtained. Efficacious application of the method, however, requires experience and a certain amount of trial and error, particularly when choosing an optimal time and spatial discretisation. Adaptive methods provide a means for obtaining more reliable solutions by continuously adjusting the discretisation in time and space according to the current solution. In geotechnical engineering, there is a wide range of nonlinear problems for which adaptivity can improve the accuracy of numerical solutions. For example, adaptive time stepping for controlling the time (load) discretisation has been used successfully to solve many geotechnical problems [1,28,29,34,35]. Automatic substepping in explicit stress integration, which adjusts the strain increment size according to the current stress state, is another form of adaptivity that has proved to be highly effective for implementing advanced constitutive models [32,36]. In contrast, adaptive spatial discretisation has attracted less attention in the field of geomechanics, perhaps because of the prevalence of the small-deformation assumption.

The FEM with adaptive spatial discretisation has been actively researched over the last three decades. A number of techniques have been developed, with the most common ones for dealing with large deformation problems being the *r*-adaptive and *h*-adaptive methods [15]. The *r*-adaptive method adjusts the spatial discretisation, but usually does not increase the overall number of elements. A classic example of this approach is the so-called Arbitrary Lagrangian–Eulerian (ALE) method. Nazem et al. [17] demonstrated the ability of this method to solve general large deformation problems in geomechanics, while Khoei et al. [12] presented an extended formulation based on the ALE technique for large deformation analysis of solid mechanics problems. Although powerful, the *r*-adaptive method does not directly address problems like localised deformation or stress concentration. The *h*-adaptive method adjusts the spatial discretisation by continuously increasing the mesh density in zones where a more accurate response is expected. This approach is particularly effective in improving the solution accuracy for problems involving large deformation, localised deformation, moving boundaries, post-failure response, steep

M. Kardani (✉) · M. Nazem · A. J. Abbo · D. Sheng · S. W. Sloan
Centre for Geotechnical and Materials Modeling,
The University of Newcastle, University Drive, Callaghan,
NSW 2308, Australia
e-mail: mina.kardani@uon.edu.au

gradients and sharp fronts. Although it is well established in solid mechanics, the *h*-adaptive FEM has attracted less attention in geomechanics with the work of Hu and Randolph [7,8] being a notable exception. As finite element analysis becomes increasingly common in geotechnical engineering, with many practical problems involving the complex features listed above, there is a pressing need for reliable methods that control the discretisation error to within a desired limit. An alternative approach to tackling the mesh distortion issue is based on the so-called meshless methods (e.g. [6,19]). However, the applicability and accuracy of these approaches for geotechnical problems are not clearly understood.

The *h*-adaptive FE strategy subdivides the integration region into successively smaller sub-regions [10], thus changing the density of the elements to yield a more accurate solution while keeping the element order constant. In the case of small deformations, where the mesh geometry does not change throughout the solution process, the *h*-adaptive method can be used to generate a better mesh at the end of the analysis with a repeated analysis being expected to improve the solution accuracy. In the literature, it is common to use the *h*-adaptive method in this way for small deformations (e.g. [2,13,24]). In the case of large deformations, where the mesh is continuously updated according to the current displacements, the *h*-adaptive method provides a natural strategy for controlling the discretisation error as the solution proceeds. The approach is thus well suited to handling problems associated with large deformations, such as mesh distortion, but reports of its use in the literature for this purpose are scarce. Another advantage is that, for the same level of accuracy, an *h*-adaptive solution is usually substantially cheaper than a conventional solution that is based on a constant (perhaps substantially higher) number of elements.

The three main components of an *h*-adaptive finite element analysis are (1) error estimation, (2) mesh generation, and (3) convection of the state variables from the old mesh to the new mesh. The error estimation procedure attempts to control the spatial discretisation error in the finite element domain which, in turn, determines the distribution of the elements in future mesh refinements. Various types of error estimators have been proposed in the literature. Residual error estimators evaluate the error by using the residuals of the approximate solution [11]. Recovery based error estimators, on the other hand, use a recovered solution instead of the exact solution to measure the error, which is usually defined in terms of some energy norm [40,41]. It is also possible to use an incremental form of error estimation based upon a global error measure in the constitutive equations [5]. The newer approach of goal-oriented error estimation is based on controlling a local quantity of interest, such as a specific displacement or stress, instead of a global quantity such as an energy norm [21,25]. After estimating the error, a criterion is needed to refine and optimise the mesh. Some well known mesh optimality criteria include Zienkiewicz and Zhu's (ZZ) procedure [39] which is based on an equal distribution of discretisation error between the elements in the current mesh, Onate and Bugeda's (OB) method [22] which is based on an equal distribution of the error density, and Li and Bettess' (LB) strategy [15] which is based on equal distribution of error in each element in the new mesh. It has been proven that the LB criterion, which is actually an improved form of the ZZ criterion, leads to the lowest number of elements and the minimum number of degrees of freedom for a given accuracy [4]. An alternative remeshing criterion can be obtained by combining the LB and the OB strategies [4].

After assessing the error, a new mesh is generated according to the refinement criterion. Then, two different approaches are available to continue the analysis. One is to restart the analysis with the new mesh from time zero. This avoids the cumbersome process of transferring variables from one mesh to another, but is only appropriate for small deformations. For large deformations, the new mesh represents the current deformed configuration and cannot be used as the initial undeformed configuration, thus making a restart of the analysis infeasible (e.g., in penetration problems such as those described by Sheng et al. [27]). An alternative strategy, which is known as remapping or convection, is to transfer the history-dependent variables and displacements from the old mesh to the new mesh. Different approaches for remapping are available in the literature such as global least square projection [20], element-based transfer which uses an extrapolation algorithm based on shape functions, and patch-based transfer or least-square approximation techniques [2]. By remapping state variables, the analysis continues with the new mesh for the next load increment. Thus, the total number of load increments is not increased, but with a cost of remapping the state variables between the old and new meshes.

Various *h*-adaptive finite element strategies can be devised by combining different forms of error estimators, mesh generators, and remapping techniques. For example, Hu and Randolph [7] proposed an *h*-adaptive finite element procedure for geotechnical problems in which the error is estimated using the Superconvergent Patch Recovery (SPR) technique to recover the strains at Gauss points. The mesh refinement procedure is based on a minimum element size criterion. To transfer the stresses and soil properties from the old mesh to the new mesh two interpolation strategies, a modified form of the unique element method and the stress-SPR method, were applied. This method has been used to analyse the bearing capacity of strip and circular foundations on non-homogeneous soil where the strength increases linearly with depth. The strategy proposed by [7] is based upon small strain analysis where the effect of rigid body rotations is neglected.

As mentioned above, the *h*-adaptive method has been used mostly for small deformation problems with only a few

studies focusing on large deformations mainly on other areas rather than geomechanics [9,23]. The key aim of previous work was to improve the accuracy of the solution, with little attention being devoted to important issues such as mesh distortion [14]. In this paper, a new and robust *h*-adaptive procedure is developed to solve nonlinear problems in geomechanics, with a particular focus on large deformations. In this approach, the error is estimated using a global energy norm, and a robust Delaunay triangulation algorithm is then employed to generate a refined mesh. Finally, all the state variables and displacement are transferred from the old mesh to the new mesh using the SPR technique. Moreover, unlike many published works in the area [7], the adaptivity concept employed in this study does not only include the mesh optimisation and refinement but also covers other important aspects of adaptivity such as automatic adaptive time stepping and adaptive stress-integration with error control. The ability of this *h*-adaptive FEM to handle complex large deformation problems is illustrated by solving some classical problems such as the bearing capacity of footings, cavity expansion and a biaxial test.

2 *h*-Adaptive FEM

Among others, the Updated-Lagrangian (UL) method is a common strategy to solve problems involved with large deformations. In the UL method the material particles are connected to a computational grid. The spatial position of this computational grid is updated according to incremental displacements at the end of each time step. Potentially, mesh distortion and entanglement of elements can occur in the material mesh due to continuous change in geometry, leading to a negative Jacobian of finite elements or a significant inaccuracy in the solution. Mesh distortion and overlapping of elements in zones with high stress and strain concentration is almost inevitable if the finite element mesh is fine enough to achieve acceptable results. This phenomenon can be observed while solving a wide range of geotechnical problems such as the bearing capacity of relatively soft soils under a footing, the penetration of objects into soil layers, the lateral movements of pipelines on seabeds, the pull-out capacity of anchors embedded in soft soils, and slope stability analysis. The h-adaptive finite element technique can eliminate the mesh distortion by, if necessary, generating an undistorted new mesh at the end of the UL analysis.

The *h*-adaptive procedure generates a sequence of approximate meshes which are aimed at either converging to a proper mesh gradually or eliminating mesh distortion in the finite element domain. In the adaptive FEM developed in this study the analysis starts with an UL step using a relatively coarse mesh over the domain of the problem. In this step, an adaptive implicit time-stepping [34] is used to solve the nonlinear global equations, during which an automatic explicit stress-integrator solves the nonlinear differential constitutive equations due to material nonlinearity. After equilibrium is reached, the nodal coordinates are updated according to the incremental displacements and the error in the finite element mesh is evaluated by an error estimator. If the error satisfies an acceptable accuracy, the analysis is continued using the same mesh in the next increment. Otherwise, the new area of each element is calculated according to the estimated error and a new mesh is generated. All state variables are then transferred from the old mesh to the new mesh and the analysis is performed using the new mesh in the next increment. This transfer process occurs at integration points as well as nodal points. In the following sections, the key components of the *h*-adaptive procedure developed, including the UL method, the error estimator, the mesh generation and remapping approach are explained in more detail.

2.1 The UL method

In the UL method it is assumed that the solution at time t is known and the main goal of the new increment is to find the state variables which satisfy equilibrium at tine $t + \Delta t$. The matrix form of the global equilibrium equation is usually derived from the principle of virtual displacements which, in its weak form, states that for any virtual displacement δu equilibrium is achieved provided

$$\int_V \sigma_{ij}\delta\varepsilon_{ij}dV = \int_V \delta u_i b_i dV + \int_S \delta u_i f_i dS \tag{1}$$

where σ denotes the Cauchy stress tensor, $\delta\varepsilon$ is the variation of strain due to virtual displacement u, b is the body force, and f is the surface load acting on area S of volume V. Linearisation of the principle of virtual displacement provides the equation of equilibrium for a solid in the following matrix form

$$K_{ep}\dot{U} = \dot{F}_{ext} \tag{2}$$

where K is the tangent stiffness matrix, U denotes the displacement vector, and F_{ext} is a vector of external forces. The solution of the equilibrium equation (2) requires a step-by-step integration scheme in an explicit or implicit form. Explicit methods, such as the central difference method, circumvent the factorization of the global matrix equation but are only conditionally stable, i.e., the size of the time steps must be smaller than a critical value. Implicit methods, on the other hand, are unconditionally stable but usually have to be combined with another procedure such as the Newton–Raphson method. In this study we adopt the time-stepping scheme with automatic subincrementation and error control proposed by Sloan and Abbo [34].

It is notable that in a large deformation analysis the constitutive equations must be objective, i.e. rigid body motion must not induce any strains in the material. In many implementations of h-adaptivity, a formulation based on multiplicative decomposition of the deformation gradient is used, together with an additive decomposition of the deformation rate which involves the definition of an intermediate stress-free configuration (e.g. [23]). This formulation originated from the micromechanical observations of metal crystals, but its application to geomaterials is yet to be investigated deeply. To address the principle of objectivity we use the Jaumann stress rate, $\sigma^{\nabla J}$, in the stress–strain relations according to

$$d\sigma_{ij}^{\nabla J} = C_{ijkl}^{ep} \cdot d\varepsilon_{kl} \tag{3}$$

where C^{ep} denotes the elastoplastic constitutive matrix. For every iteration in which plastic yielding occurs, the nonlinear differential equation in (3) needs to be solved at each integration point inside the mesh. An explicit automatic stress-integration scheme with error control was developed by Sloan [32] and refined by Sloan et al. [36] for this purpose. Nazem et al. [18] successfully extended this scheme to large deformation problems of solid mechanics and demonstrated that it is slightly more efficient to apply rigid body corrections during integration of the constitutive equations. This adaptive stress-integration scheme is adopted in this study.

2.2 Error estimator

Since an exact solution is usually not available, an approximate error assessment is used to guide the mesh refinement. During the error assessment, the error in each element is calculated and compared with a prescribed limit, thus identifying parts of the domain where the discretisation needs refinement. The error estimation method implemented in the present work is based on that of Boroomand and Zienkiewicz [2], and uses the energy norm for nonlinear elasto-plasticity. The error in an increment is calculated using

$$\|e\| = \left[\int_{\Omega} |(\sigma - \hat{\sigma})^T (\Delta\varepsilon - \Delta\hat{\varepsilon})| d\Omega \right]^{\frac{1}{2}} \tag{4}$$

where $\Delta\varepsilon$ and $\Delta\hat{\varepsilon}$ represent the exact and the finite element strain increments, σ and $\hat{\sigma}$ denote the exact and finite element approximation of the stresses, and Ω is the problem domain. To estimate the error, the exact stress and strain fields are replaced by their recovered values, σ^* and $\Delta\varepsilon^*$, which are calculated using the SPR procedure. This means that Eq. (4) becomes

$$\|e^*\| = \left[\int_{\Omega} |(\sigma^* - \hat{\sigma})^T (\Delta\varepsilon^* - \Delta\hat{\varepsilon})| d\Omega \right]^{1/2} = \left[\sum_{i=1}^{nel} \|e_{el}^*\|_i \right]^{1/2} \tag{5}$$

where nel is the total number of elements and $\|e_{el}^*\|$ represents the estimated error in each element defined by

$$\|e_{el}^*\| = \sum_{i=1}^{ngp} w_i (\sigma_i^* - \hat{\sigma}_i)^T (\Delta\varepsilon_i^* - \Delta\hat{\varepsilon}_i) \tag{6}$$

In the above, ngp is the total number of Gauss points in an element and w_i is the standard Gauss quadrature weight. The relative error in the solution based on the incremental energy norm can be obtained by

$$\eta = \frac{\|e^*\|}{E} \times 100 \tag{7}$$

where

$$E = \left(\sum_{j=1}^{nel} \sum_{i=1}^{ngp} w_i \sigma_{ji}^{*T} \Delta\varepsilon_{ji}^* \right)^{1/2} \tag{8}$$

This error is then compared with a prescribed accuracy, $\bar{\eta}$ according to

$$\eta \leq \overline{\eta} \tag{9}$$

If the condition (9) is satisfied, no further refinement is needed. Otherwise, we assume that the error is equally distributed over the elements and use the LB criterion to obtain the new element area:

$$A_{new} = \left(\frac{\overline{\eta} E}{\|e_i^*\| \sqrt{N}} \right)^{1/p} \times A_{old} \tag{10}$$

in which N represents the total number of elements in the old mesh and p is the polynomial order of the approximation. Since this method estimates the error using a global quantity, the energy norm, it cannot be used to control the error in local quantities of interest, such as a specific component of stress or strain.

2.3 Mesh generation

Mesh generation algorithms fall into two broad categories: structured and unstructured. A structured mesh generator produces elements with regular connectivity that can be expressed as a two- or three-dimensional array. In this approach the nodes are located directly using a variety of methods including specified functions, simple algorithms such as the Laplacian operator, or by manually decomposing the problem domain into simple patches. Unstructured mesh

generators, on the other hand, are often boundary based and typically require some form of boundary discretisation to be specified. In every step of the element generation, the geometry of the unmeshed region is assessed and the boundary definition is preserved. Unstructured meshes are characterized by irregular connectivity, and are efficient in the sense that they permit elements to be highly concentrated in zones where they are needed. For 2D applications the Delaunay triangulation (DT) (see, e.g. [33]) is probably the most popular unstructured mesh generation method. A key feature of this method is that the circumcircle/circumsphere of every triangle/tetrahedron does not contain any other nodal points of the triangulation. Moreover, in 2D it can be shown that the DT maximises the minimum angle in any triangle, thereby guaranteeing high quality grids for computational work.

In this paper the mesh generation is based on a program named *Triangle* [31] which takes advantage of various existing Delaunay triangulation algorithms to generate high quality meshes for two-dimensional domains. The program is a fast and robust tool to construct Delaunay triangulations, constrained Delaunay triangulations and Voronoi diagrams. In this code, Ruppert's Delaunay refinement algorithm is used to check that no angle in any triangle is allowed to be smaller than 20°. The availability of *Triangle*'s source code made it possible to apply new changes to the code. In this work, significant improvements have been made to *Triangle,* to make it compatible with the requirements of this study. For example, keeping track of the previous stage of the mesh for the refinement procedure, dealing with problems involving large deformation by constantly changing the domain, constraining the minimum element area, and introducing regions with different maximum and minimum areas. Also, the order of the generated nodes is optimised to minimise the memory allocation and CPU time, with mesh distortion being avoided during the refinement procedure.

2.4 Remapping

After generating the new mesh based on the estimated error, all state variables at Gauss points and nodal points need to be transferred from the old mesh to the new mesh. Nodal variables can be transferred from the old nodes to the new nodes by a direct interpolation. If the new coordinates of a node match the old coordinates of a node the displacements remain unchanged, but if a new node is generated on a segment with a prescribed displacement it will inherit the characteristics of that segment. The displacements of all other new nodes are found simply by using the displacement shape functions of the surrounding old element.

Transferring the information from old Gauss points to the new Gauss points is less straightforward, as it can lead to a loss of equilibrium and violation of the yield condition. In this work, the super convergent patch recovery technique [40,41] is used to compute the nodal quantities of interest (such as stresses). This technique has been successfully used with h-adaptive as well as r-adaptive FEMs [7,17], and assumes that the quantities in a patch can be modelled using a polynomial of the same order as the displacements. Thus, for two-dimensional quadratic elements, the stresses over a patch may be written as

$$\sigma = P \cdot a \tag{11}$$

where

$$P = [1, x, y, x^2, xy, y^2] \tag{12}$$

and

$$a = [a_1, a_2, a_3, a_4, a_5, a_6]^T \tag{13}$$

In Eq. (12), normalised coordinates are used instead of global coordinates to avoid ill-conditioning of equations for higher order elements. The normalised coordinates in a two-dimensional patch, x_i^* and y_i^*, can be written as

$$\begin{aligned} x_i^* &= -1 + 2\frac{x_i - x_{\min}}{x_{\max} - x_{\min}} \\ y_i^* &= -1 + 2\frac{y_i - y_{\min}}{y_{\max} - y_{\min}} \end{aligned} \tag{14}$$

in which $x_{\min}$ and $x_{\max}$ represent the maximum and minimum values of the x-coordinates in the patch, respectively, and $y_{\max}$ and $y_{\min}$ are defined similarly for the y-coordinates. A least squares fit is then used to find the unknown values of a by minimising

$$F(a) = \sum_{i=1}^{m} (\sigma(x_i^*, y_i^*) - P(x_i^*, y_i^*) \cdot a)^2 \tag{15}$$

in which $\sigma(x_i^*, y_i^*)$ are the stress values at Gauss points and m is the number of Gauss points in a patch. This defines a according to

$$a = A^{-1} b \tag{16}$$

where

$$A = \sum_{i=1}^{m} P^T(x_i^*, y_i^*) P(x_i^*, y_i^*) \tag{17}$$

$$b = \sum_{i=1}^{m} P^T(x_i^*, y_i^*) \sigma(x_i^*, y_i^*) \tag{18}$$

The stresses at any node or Gauss point in the new mesh are obtained by substituting the normalised coordinates in Eq. (11) for the surrounding patch in the old mesh. As the topology of the mesh can change, it is possible to find more than one enclosed patch for a specific Gauss point or node. In this case, the final value of the stresses is set equal to the mean of the calculated stresses in each patch.

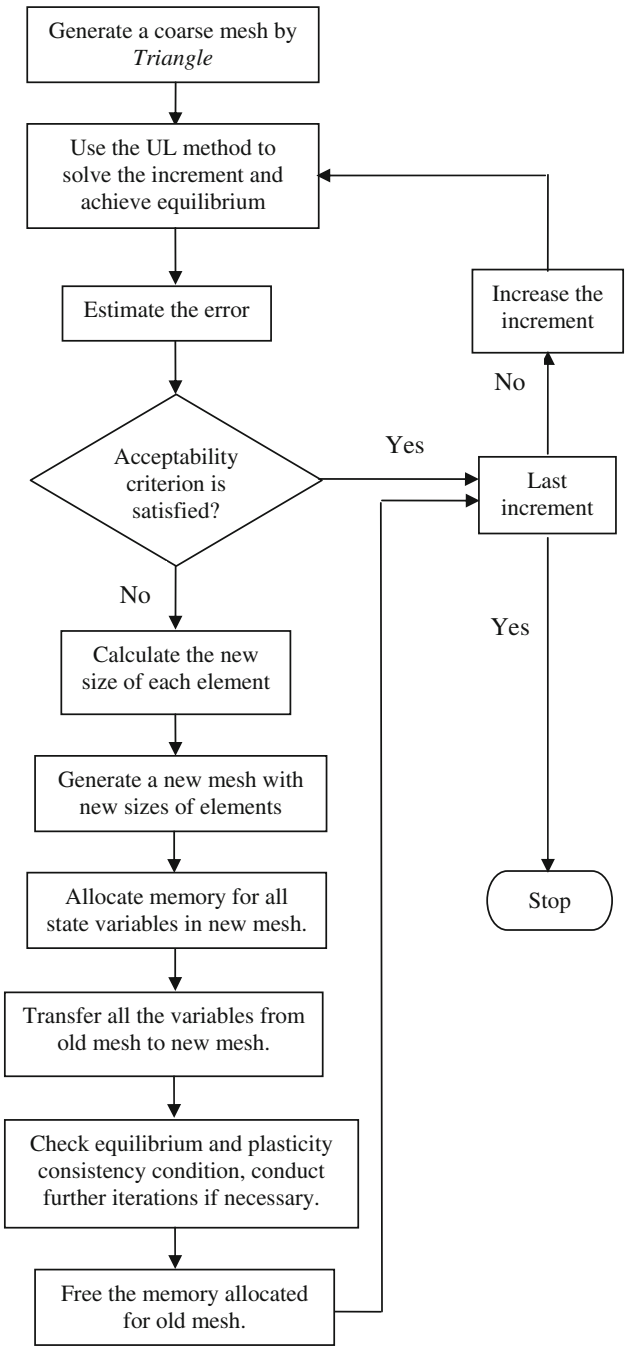

Fig. 1 Procedure for h-adaptive finite element analysis

2.5 Implementation of the *h*-adaptive algorithm

The components of the *h*-adaptive FEM described in the above sections have been implemented into SNAC, a finite element program developed over the past two decades by the geotechnical research group at the University of Newcastle, Australia. The algorithm is shown schematically in Fig. 1.

In the *h*-adaptive procedure, the analysis starts with *Triangle* to generate a coarse mesh on the domain based upon the user information. It is possible to define the maximum area of elements in each region. In the data given by the user, the domain of the problem is defined by a combination of points and segments. Each point represents the intersection of two segments and a segment can be either a straight line or a curve. The domain of the problem may consist of several regions.

In the first increment, the global nonlinear equations are solved to find the incremental displacements and consequent incremental strains. The constitutive equations are then integrated to obtain the stresses. After finding the stresses, the analysis continues by calculating the internal forces and checking equilibrium. The error in the current mesh is then calculated based on the error in the global energy norm and the program checks if this error is acceptable. For all elements where the estimated error is above a specified tolerance, a new area is assigned to minimise the error. The old mesh is then refined according to the new element sizes. After generating the new mesh, all the state parameters are transferred from the old mesh to the new mesh. Since the topology of the new mesh is potentially different to the topology of the old mesh, the code must store the information of two meshes in memory simultaneously, demanding a precise memory reallocation routine. This information must include the total number of nodes and their spatial coordinates, the number of elements and their connectivity, the boundary conditions, the applied loading, and all state variables at the Gauss points.

For elastoplastic materials, the remapped state variables may violate the equilibrium and yield conditions in the new mesh. Ideally, transferring the state variables from an old mesh to a new mesh should not cause any straining and hence equilibrium should still be satisfied. Moreover, the remapped stresses must lie inside or on the yield surface. Unfortunately, there is no simple way to satisfy these two conditions simultaneously and the development of a rigorous algorithm for remapping remains a challenge. In this work, if a stress point is found to lie outside the yield surface after remapping, it is projected back to the yield surface using the stress correction procedure described in Sloan et al. [36]. After these corrections are executed, equilibrium is enforced by conducting additional iterations at the global level (if needed).

In some stages of the process it may be observed that further refinement may not improve the results and also lead to mesh distortion due to the generation of very small elements. To avoid this problem, a minimum element area is prescribed for every region inside the meshed domain. This guarantees that the area of each individual element will not be smaller than a minimum value, even if the associated error estimator indicates otherwise. In addition, the solution algorithm can terminate the mesh refinement at any time-step, thus allowing the analysis to be continued with the last generated mesh for the remaining load increments.

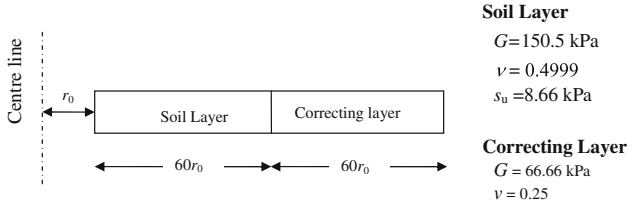

Fig. 2 The cavity expansion problem (geometry not to scale)

3 Numerical examples

In this section, the h-adaptive FEM described above is used to solve some classical geotechnical problems. Problems considered include the expansion of a cylindrical cavity, a biaxial test, and the bearing capacity of a flexible as well as a rigid footing. All problems have been solved using 6-node triangular elements with six integration points and analysed assuming large deformation.

3.1 Elastoplastic cylindrical cavity expansion

The cavity expansion problem in a Tresca soil is one of the few cases that can be solved analytically using finite-strain plasticity, and is thus very useful for validating finite element formulations. The internal radius of the cavity is denoted as a_0 while the outer radius is set to $60r_0$. To simulate the effects of an infinite medium, a correcting elastic layer is added to the soil layer [3]. Figure 2 represents the boundary conditions, material properties, and the finite element mesh of the cavity used in this analysis. In Fig. 2, G, s_u, and v represent the shear modulus, undrained shear strength, and Poisson's ratio of the soil, respectively. A total prescribed radial displacement of magnitude $6r_0$ is applied over 200 equal time increments. The analytical solution according to Yu [38] is:

$$\frac{\Psi}{s_u} = 1 + \ln\left[\frac{G}{s_u}\left(1 - \frac{r_0^2}{r^2}\right) + \frac{r_0^2}{r^2}\right] \tag{19}$$

where Ψ represents the internal pressure of the cavity and r is the current internal radius of the cavity. The numerical solution for the normalised internal pressure of the cavity versus the normalised radial displacement is compared with the analytical solution in Fig. 3. Good agreement between the analytical and the numerical solutions is observed.

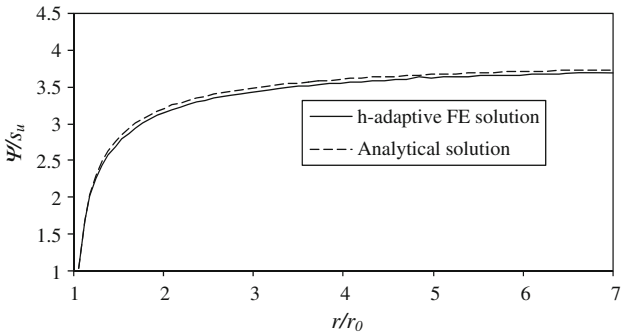

Fig. 3 Normalised internal pressure of cavity versus normalised radial displacement

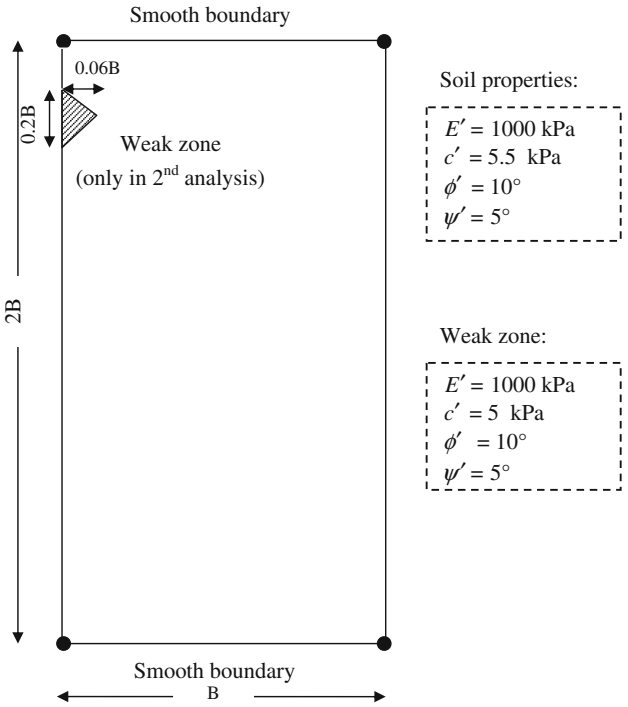

Fig. 4 Biaxial test (Sect. 3.2)

3.2 Biaxial test

In this example, a biaxial test is simulated using the Mohr–Coulomb criterion with a non-associated flow rule. The problem is solved using two different material properties. First a uniform soil layer is considered for the entire domain. Then, localised failure is initiated by defining weaker properties for a small area in the soil specimen. The geometry of the problem, material properties and boundary conditions are shown in Fig. 4. The soil is modelled using a rounded Mohr–Coulomb model proposed by Sheng et al. [30]. In Fig. 4, E', c', ϕ', ψ' and B represent the drained Young's modulus, the drained cohesion, the drained friction angle of the soil, the dilation angle and the width of the specimen, respectively.

A total axial strain of 7% is applied vertically on the specimen, in 100 equal increments. Figure 5 shows the initial meshes, the meshes at the increments 10 and 20 for the uniform soil properties, and the meshes at the increments 20 and 40 for the non-uniform soil properties with a minimum element area of $0.00016B^2$. For comparison, the problem was reanalysed by using a very fine fixed mesh with 7,763 elements and 15,768 nodes considering both uniform and

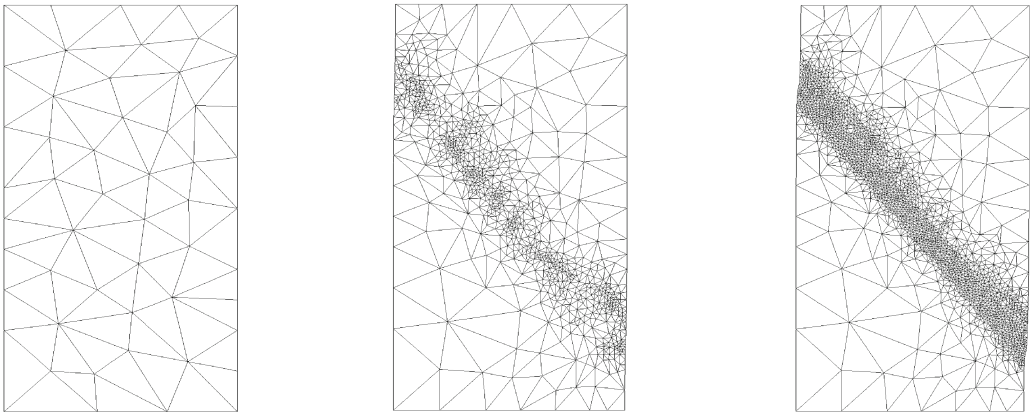

1) Coarse mesh (80 elements) 2) After 10 remeshing (731 elements) 3) After 20 remeshing (1658 elements)

(a) Uniform soil properties

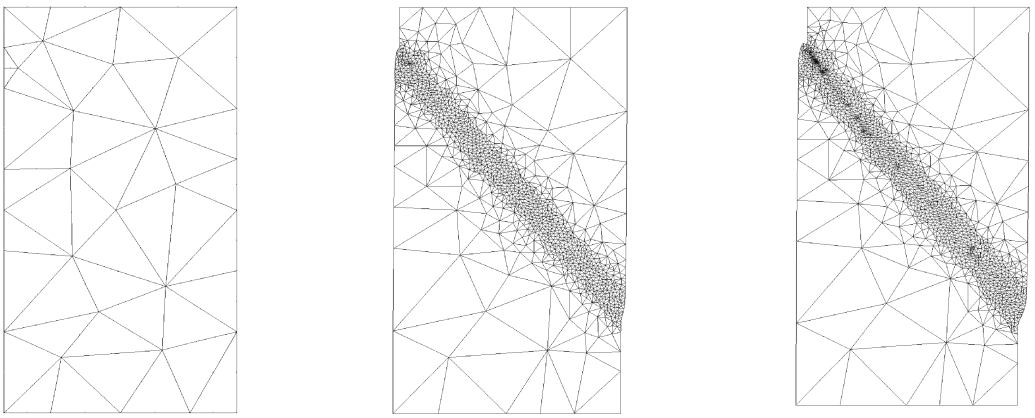

1) Coarse mesh (47 elements) 2) After 20 remeshing (2337 3) After 40 remeshing (2792 elements)

(b) Non-uniform soil properties

Fig. 5 Mesh results of the biaxial tests

non-uniform soil properties. The applied pressure normalized by c' is plotted versus the axial strain in Fig. 6 for both the adaptive mesh and the fixed fine mesh in each analysis. Obviously, analysis using a fixed mesh does not locate the shear band. However as shown in Fig. 7, the h-adaptive method can predict the location and formation of the shear band in this problem. To demonstrate the effect of prescribing larger minimum element areas on the accuracy of the solution, both problems are also analysed with minimum area of $0.0032B^2$ and $0.00032B^2$. As shown in Fig. 6, reducing the size of the minimum element area increases the accuracy of the solution. Moreover, the load–deflection curve does not change for the values of minimum element area less than about $0.00016B^2$, which implies that no further mesh refinement is necessary when an element size reaches this value. Also, by increasing the number of elements in a very fine structured mesh, the solution remains unchanged and convergence is evident.

It is interesting to note that the continuous mesh refinement leads to a thinner and thinner shear band. However, the load–displacement curves shown in Fig. 6 indicate convergence to a unique solution, i.e., the load deflection behaviour does not change significantly with the density of the initial mesh as long as the analysis begins with a reasonably coarse mesh. Runesson et al. [26] showed that introducing some softening to the associated model, or using a non-associated flow rule, would also permit bifurcation. In general, a more robust alternative for tackling this localisation problem would be to combine the proposed adaptive method with an appropriate constitutive model for the localisation [16,37].

3.3 Bearing capacity of soil under a strip footing

In the third example, a strip footing on an undrained soil layer of Tresca material is considered. Only half of the footing

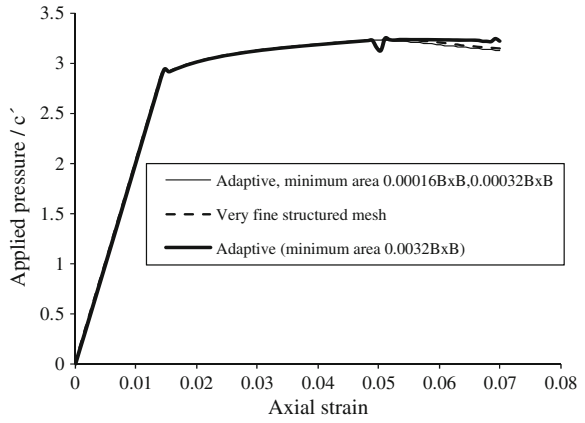

(a) Uniform soil properties

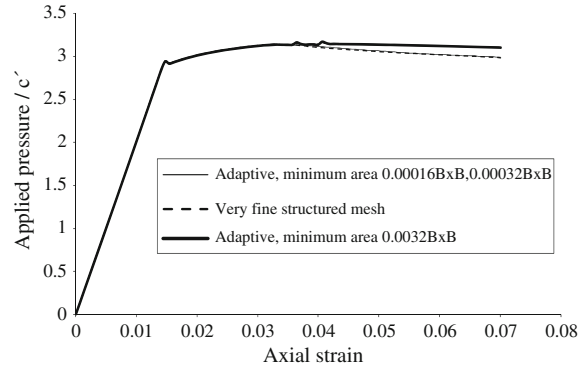

(b) Non-uniform soil properties

Fig. 6 Load–displacement response of the biaxial test

is analysed due to symmetry, and the domain, its boundary conditions and material properties are shown in Fig. 8. The footing is assumed to be either flexible or rigid.

To model a flexible load, a vertical pressure $6.5s_u$ is applied to the footing in 200 equal time steps. The domain is analysed using two different finite element meshes: a very fine mesh and a relatively coarse mesh. The coarse mesh has only 299 elements and a maximum element area of $0.25B^2$, while the fine mesh has 3,713 elements and a maximum element area of $0.02B^2$. Table 1 provides the minimum element area, number of nodes, number of elements and the consumed CPU time in each analysis. The topology of the domain is kept constant in the fine mesh, while the coarse mesh is refined continuously using the h-adaptive technique. The number of nodes and the elements in the h-adaptive analysis provided in Table 1 correspond to those at the end of analysis. The h-adaptive solution was found using a total of 32 mesh refinements. The evolution of the adaptive mesh shown in Fig. 9 indicates the finite element meshes at the beginning of the analysis and after 10, 25 and 30 mesh refinements, respectively. This figure clearly shows that the h-adaptive method is able to predict the occurrence and location of the shear band under the footing successfully. Figure 9 plots the applied pressure on the footing, normalised with respect to s_u, versus the vertical displacement normalised with respect to the half width of the footing. The results presented in Fig. 10 are based upon the assumption of large deformations, i.e., the limit pressure does not necessarily converge to Prandtl's plasticity solution, $(2+\pi)s_u$. The two load–displacement plots

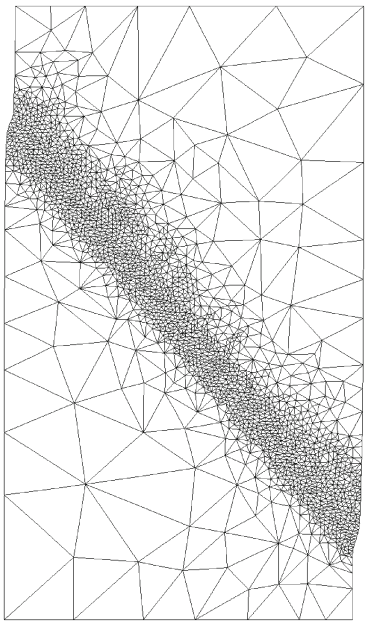

(a) uniform soil properties (2964 elements and 6001 nodes)

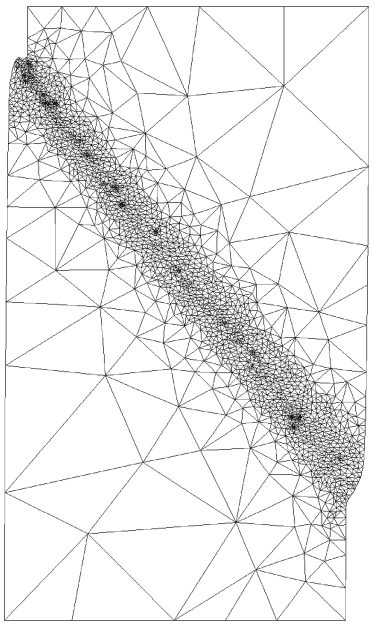

(b) Non-uniform soil properties (3363 elements and 6802 nodes)

Fig. 7 Final deformed h-adaptive meshes for biaxial test

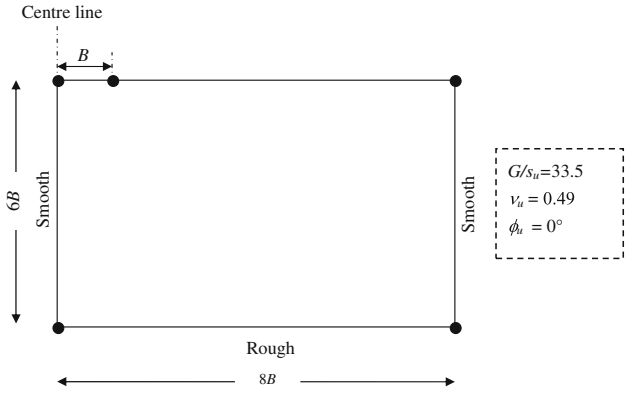

Fig. 8 Footing problem

coincide perfectly with each other, while the *h*-adaptive analysis is approximately 14 times faster than the analysis using the fixed fine mesh (Table 1). In another attempt to solve this example, a minimum element area of $0.01B^2$ was selected and no mesh refinement was permitted. As a result, a new fine mesh with 15,168 nodes and 7,467 elements lead to almost an identical load–displacement curve as shown in Fig. 10. On the other hand, a fixed mesh with less than 1,000 elements would lead to significantly different load–displacement response. Figure 11 shows the final deformed mesh at the end of analysis. Again, the localised failure mechanism is well captured.

Table 1 Results for analysis of flexible strip footing

Analysis	Minimum element area (B^2)	Number of nodes	Number of elements	CPU time (s)
Very fine	0.02	7,604	3,713	8,013
H-adaptive				
Initial	0.25	648	299	589
Final	0.002	2,132	1,025	

For the case of a rigid footing, a vertical displacement of $0.5B$ is applied to the footing in 100 equal steps. The problem is analysed as a large deformation formulation, with some intermediate meshes being shown in Fig. 12. The final result is achieved after 32 remeshing steps. For comparison, the problem is also analysed by a small deformation assumption where the configuration remains unchanged during the

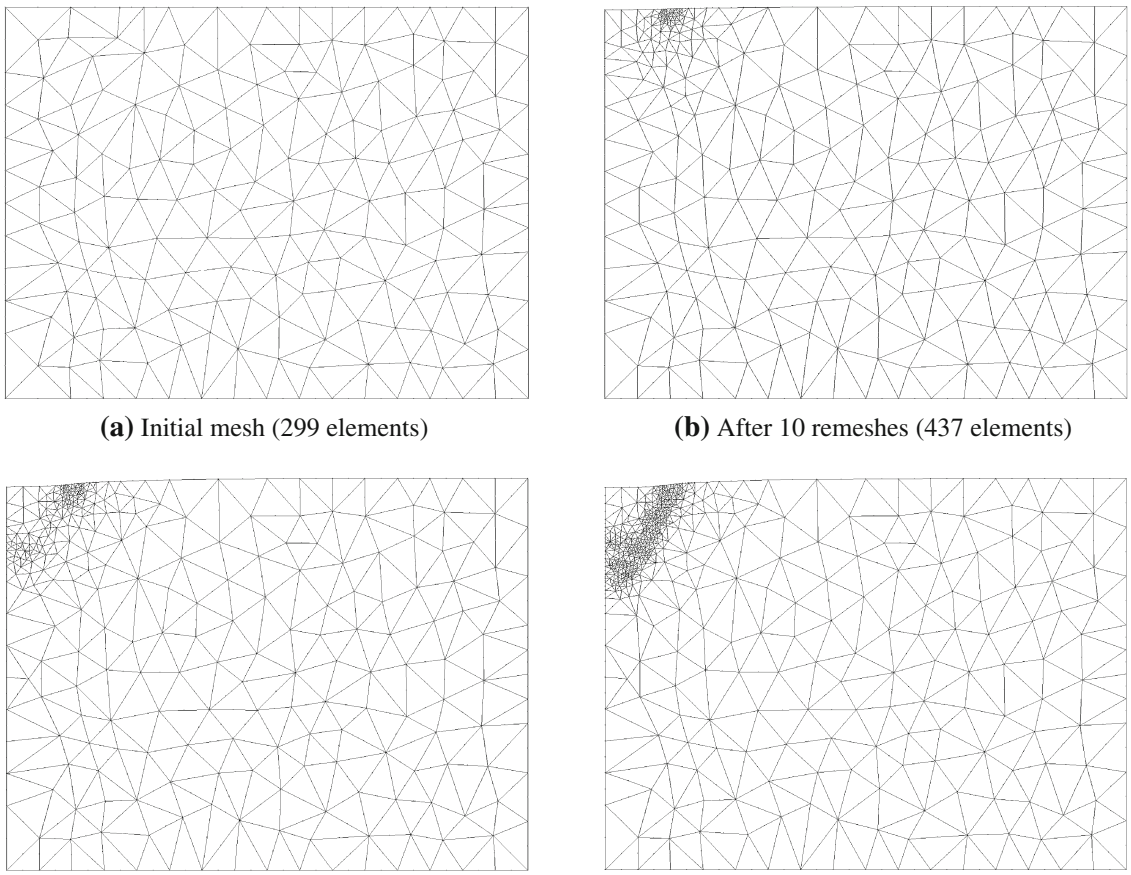

(a) Initial mesh (299 elements)

(b) After 10 remeshes (437 elements)

(c) After 25 remeshes (539 elements)

(d) After 30 remeshes (888 elements)

Fig. 9 Finite element mesh during analysis of flexible strip footing

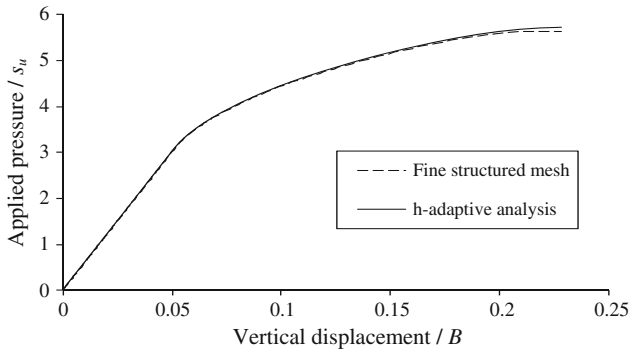

Fig. 10 Load–displacement response of flexible footing

analysis. Figure 13 plots the applied pressure on the footing, normalised with respect to s_u, versus the vertical displacement, normalised with respect to the half width of the footing. To study the effect of minimum element area, the analysis is also performed using minimum element areas of $0.001B^2$ and $0.05B^2$. As shown in Fig. 13, values of the minimum element area less than $0.002B^2$ do not increase the accuracy of the solution.

The small deformation analysis results in a final applied pressure of $5.18s_u$ which is 0.8% above Prandtl's plasticity solution of $(2+\pi)s_u$. The final deformed mesh at the end of h-adaptive large deformation analysis is shown in Fig. 14.

Fig. 11 Final deformed mesh for flexible strip footing

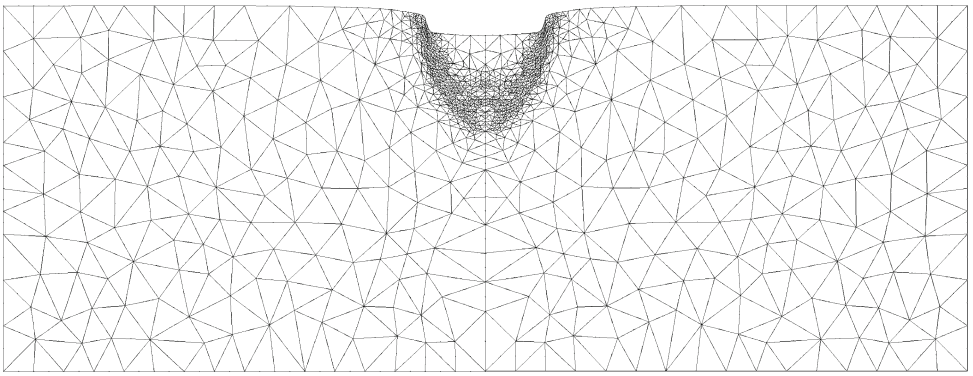

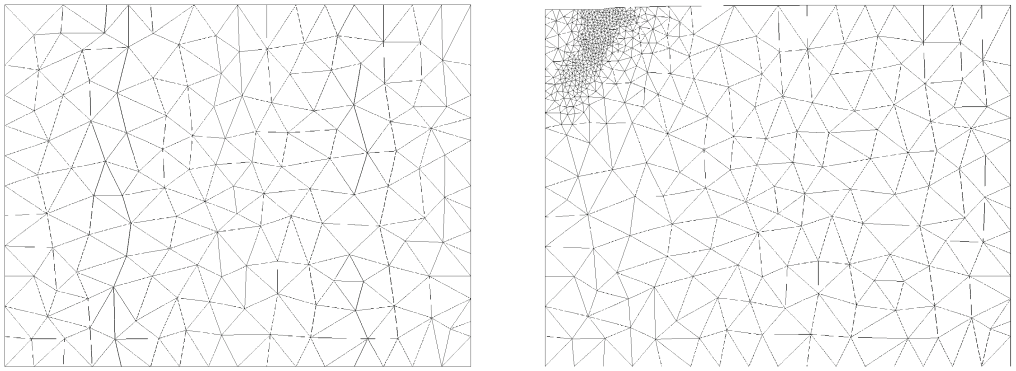

(a) Initial mesh (300 elements)

(b) After 10 remeshes (1103 elements)

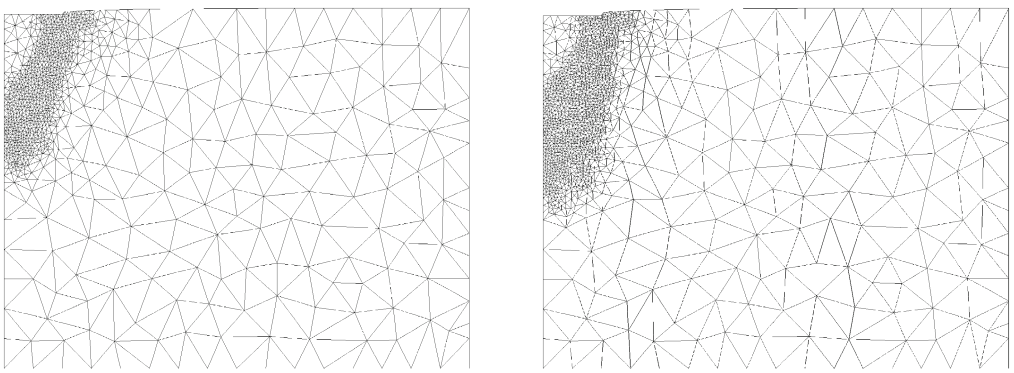

(c) After 15 remeshes (1730 elements)

(d) After 20 remeshes (2143 elements)

Fig. 12 Finite element meshes during analysis of rigid strip footing

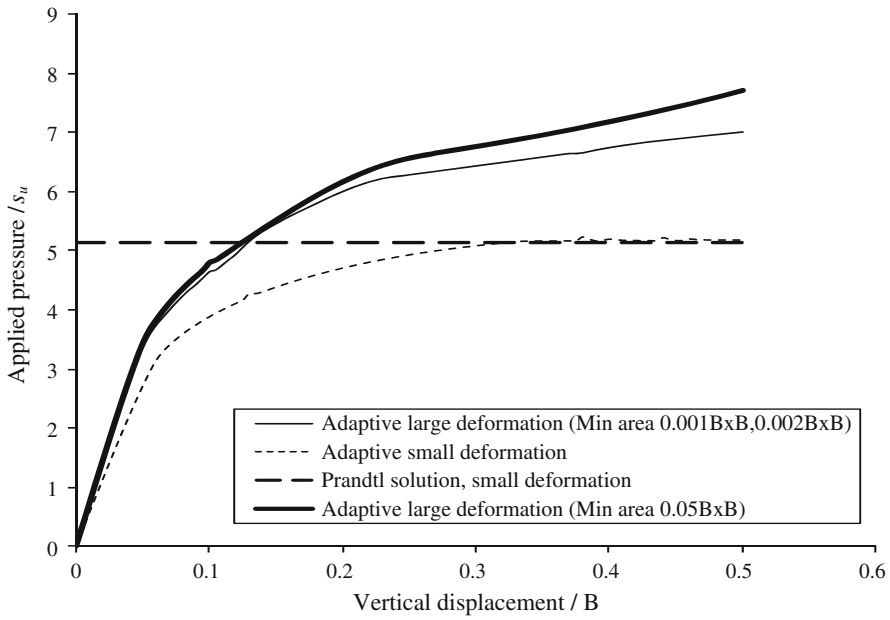

Fig. 13 Load–displacement response of rigid strip footing

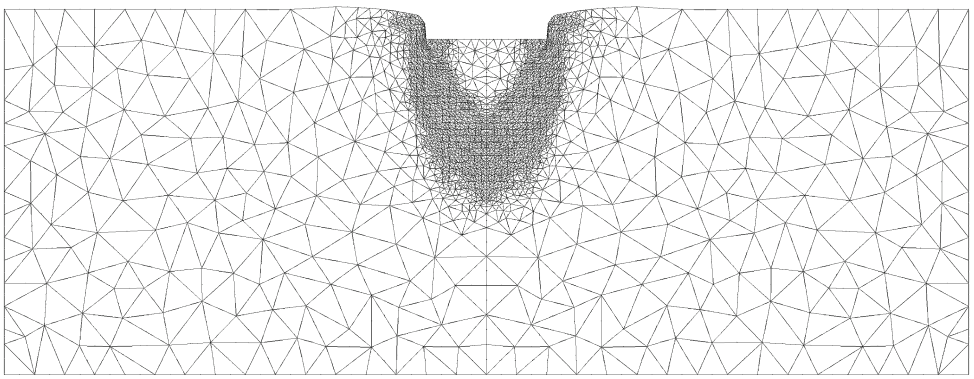

Fig. 14 Final deformed mesh for rigid footing

4 Conclusion

The *h*-adaptive FEM presented here is able to solve a wide range of nonlinear geotechnical problems efficiently and accurately. It is particularly effective in capturing localised failure and shear bands, which are difficult to predict using fixed grids. The problems analysed in this paper involve large deformations. This *h*-adaptive technique also seems to be quite efficient in dealing with problems involving large deformation, where mesh distortion can affect the accuracy of the solution. In terms of efficiency, the *h*-adaptive technique is able to produce accurate results with considerably less numbers of elements and nodes and significantly less computational time.

References

1. Allix O, Kerfriden P, Gosselet P (2010) On the control of the load increments for a proper description of multiple delamination in a domain decomposition framework. Int J Numer Methods Eng 83:1518–1540
2. Boroomand B, Zienkiewicz OC (1999) Recovery procedures in error estimation and adaptivity. Part II. Adaptivity in nonlinear problems of elasto-plasticity behaviour. Comput Methods Appl Mech Eng 176:127–146
3. Burd HJ (1986) A large displacement finite element analysis of a reinforced unpaved road. PhD Thesis. Oxford University, England
4. Diez P, Huerta A (1999) A unified approach to remeshing strategies for finite element h-adaptivity. Comput Methods Appl Mech Eng 176:215–229
5. Gallimard L, Ladeveze P, Pelle JP (1996) Error estimation and adaptivity in elastoplasticity. Int J Numer Methods Eng 46: 189–217
6. Heaney CE, Augarde CE, Deek AJ (2010) Modelling elasto-plasticity using the hybrid MLPG method. Comput Model Eng Sci 56:153–178
7. Hu Y, Randolph MF (1998) H-adaptive FE analysis of elasto-plastic non-homogeneous soil with large deformation. Comput Geotech 23:61–83
8. Hu Y, Randolph MF (1999) Plate-penetrometer penetration into NC soil using h-adaptive FE method. In: Proceedings of NUMOG VII international symposium on numerical models in geomechanics, A.A. Balkema, The Netherlands, pp 501–506

9. Hu G, Wriggers P (2002) On the adaptive finite element method of steady-state rolling contact for hyperelasticity in finite deformation. Comput Methods Appl Mech Eng 191:1333–1348
10. Huerta A, Rodriguez-Ferran A, Diez P, Sarrate J (1999) Adaptive finite element strategies based on error assessment. Int J Numer Methods Eng 46:1803–1818
11. Huerta A, Diez P (2000) Error estimation including pollution assessment for nonlinear finite element analysis. Comput Methods Appl Mech Eng 181:21–41
12. Khoei AR, Anahid M, Shahin K (2008) An extended arbitrary Lagrangian–Eulerian finite element method for large deformation of solid mechanics. Finite Elements Anal Des 44:401–416
13. Khoei AR, Gharehbaghi SA, Tabarraie AR, Riahi A (2007) Error estimation, adaptivity and data transfer in enriched plasticity continua to analysis of shear band localization. Appl Math Model 31:983–1000
14. Khoei AR, Lewis RW (2002) H-adaptive finite element analysis for localization phenomena with reference to metal powder forming. Finite Elements Anal Des 38:503–519
15. Li LY, Bettess P (1997) Adaptive finite element methods: a review. Appl Mech Rev 50:581–591
16. Mühlhaus HB, Vardoulakis I (1987) The thickness of shear bands in granular materials. Geotechnique 37:271–283
17. Nazem M, Sheng D, Carter JP (2006) Stress integration and mesh refinement for large deformation in geomechanics. Int J Numer Methods Eng 65:1002–1027
18. Nazem M, Carter JP, Sheng D, Sloan SW (2009) Alternative stress-integration schemes for large-deformation problems of solid mechanics. Finite Elements Anal Des 45(12):934–943
19. Nguyen VP, Rabczuk T, Bordas S, Duflot M (2008) Meshless methods: a review and computer implementation aspects. Math Comput Simul 79:763–813
20. Oden JT, Brauchli HJ (1971) On the calculation of consistent stress distributions in finite element approximation. Int J Numer Methods Eng 3:317–325
21. Oden JT, Prudhomme S (2001) Goal-oriented error estimation and adaptivity for the finite element method. Comput Math Appl 41:735–756
22. Onate E, Bugeda G (1993) A study of mesh optimality criteria in adaptive finite element analysis. Eng Comput 10:307–321
23. Peric D, Vaz M Jr, Owen DRJ (1999) On adaptive strategies for large deformations of elasto-plastic solids at finite strains: computational issues and industrial applications. Comput Methods Appl Mech Eng 176:279–312
24. Rannacher R, Suttmeier FT (1999) A posteriori error estimation and mesh adaptation for finite element models in elasto-plasticity. Comput Methods Appl Mech Eng 176:333–361
25. Rieger A, Wriggers P (2000) Comparison of different error estimators for contact problems. Eng Comput 17:255–273
26. Runesson K, Ottosen NS, Peric D (1991) Discontinuous bifurcations of elastic-plastic solutions at plane stress and plane strain. Int J Plast 7:99–121
27. Sheng D, Nazem M, Carter JP (2009) Some computational aspects for solving deep penetration problems in geomechanics. Comput Mech 44:549–561
28. Sheng D, Sloan SW (2001) Load stepping schemes for critical state models. Int J Numer Methods Eng 50(1):67–93
29. Sheng D, Sloan SW (2003) Time stepping schemes for coupled displacement and pore pressure analysis. Comput Mech 31: 122–134
30. Sheng D, Sloan SW, Yu HS (2000) Aspects of finite element implementation of critical state models. Comput Mech 26:185–196
31. Shewchuk JR (1996) Triangle: engineering a 2D quality mesh generator and Delaunay triangulator, Applied Computational Geometry: Toward Geometric Engineering. Lecture Notes in Computer Science, vol 1148. Springer, Berlin, pp 203–222
32. Sloan SW (1987) Substepping schemes for the numerical integration of elastoplastic stress–strain relations. Int J Numer Methods Eng 24(5):893–911
33. Sloan SW (1993) A fast algorithm for generating constrained Delaunay triangulations. Comput Struct 47:441–450
34. Sloan SW, Abbo AJ (1999) Biot consolidation analysis with automatic time stepping and error control. Part 1. Theory and implementation. Int J Numer Anal Methods Geomech 23:467–492
35. Sloan SW, Abbo AJ (1999) Biot consolidation analysis with automatic time stepping and error control. Part 2. Applications. Int J Numer Anal Methods Geomech 23:493–529
36. Sloan SW, Abbo AJ, Sheng D (2001) Refined explicit integration of elastoplastic models with automatic error control. Eng Comput 18:121–154, Erratum: Eng Comput 19(5/6):594–594, 2002
37. Tejchman J, Bauer E (1996) Numerical simulation of shear band formation with a polar hypoplastic constitutive model. Comput Geotech 19(3):221–244
38. Yu HS (2000) Cavity expansion methods in geomechanics. Kluwer Academic Publishers, The Netherlands
39. Zienkiewicz OC, Zhu JZ (1987) A simple error estimator and adaptive procedure for practical engineering analysis. Int J Numer Methods Eng 24:337–357
40. Zienkiewicz OC, Zhu JZ (1992) The superconvergent patch recovery and a posteriori error estimate. Part I. The recovery technique. Int J Numer Methods Eng 33:1331–1364
41. Zienkiewicz OC, Zhu JZ (1992) The superconvergent patch recovery and a posteriori error estimate. Part II. Error estimates and adaptivity. Int J Numer Methods Eng 33:1365–1382